Vol. 17, No. 3 (2018) 1159-1172
Revista Mexicana de Ingeniería Química

EFFECT OF ALKALINITY VARIATION IN GEL COMPOSITION DEVELOPED FOR HIERARCHICAL ZSM-5 GROWTH: CONVERSION OF ZSM-5 TO MORDENITE

EFECTO DE LA VARIACIÓN DE LA ALCALINIDAD EN LA COMPOSICIÓN DEL GEL DESARROLLADO PARA EL CRECIMIENTO DE ZSM-5 CON ESTRUCTURA JERÁRQUICA: CONVERSIÓN DE ZSM-5 A MORDENITA

R.I. Yocupicio-Gaxiola*, V. Petranovskii, J. Antúnez-García, T.A. Zepeda, S. Fuentes
Centro de Nanociencias y Nanotecnología, Universidad Nacional Autónoma de México, Ensenada, Baja California, C.P. 22860, México.

Received December 17, 2017; Accepted April 28, 2018

Abstract

In the synthesis of mesoporous hierarchical material based on MFI zeolite in the presence of mesoporogen agents, it was revealed that variations in alkalinity and Na_2O/SiO_2 ratios lead to cardinal changes in the structure of the zeolite. Although the original composition was designed to synthesize MFI in the presence of a specific organic SDA agent, a MOR phase appeared, very poor in Al. Since the synthetic mixtures used do not have a sufficient amount of Al for the synthesis of MOR in the solution, the Si/Al ratio of the obtained MOR (11) phase differs significantly from the typical one (5). A series of samples were obtained, starting with MFI, through MFI/MOR mixtures, completely MOR phases and finally amorphous mesoporous material. The molar ratio of Na_2O/SiO_2 dictates the type of zeolite structure, which makes it clear that the specific structure of the zeolite (MOR) will be formed regardless of the use of the organic SDA agent intended for the growth of another zeolite (MFI).

Keywords: mordenite; ZSM-5; hierarchical; mesoporosity; lamellar.

Resumen

En la síntesis de un material jerárquico mesoporoso basado en zeolita ZSM-5 (MFI) en presencia de agentes mesóporogenos, se reveló que las variaciones en la alcalinidad y las relaciones Na_2O/SiO_2 conducen a cambios cardinales en la estructura de la zeolita. La presencia de un agente director de estructura (SDA) orgánico en la síntesis de MFI dio lugar a la coexistencia de ZSM-5 con una fase de mordenita, muy pobre en Al. Debido a que no hay suficiente Al para la síntesis de mordenita en la solución, la relación Si/Al fue de 11 en la MOR obtenida la cual difiere significativamente de la típica de 5. Se obtuvo una serie de muestras, comenzando con MFI, a través de mezclas MFI/MOR, fases completamente MOR y finalmente material mesoporoso amorfo. La relación molar de Na_2O/SiO_2 determina el tipo de estructura de zeolita, lo que deja en claro que la estructura específica de la zeolita (MOR) se formará independientemente del uso del agente orgánico SDA destinado al crecimiento de otra zeolita (MFI).

Palabras clave: mordenita; ZSM-5; jerárquica; mesoporosidad; laminar.

1 Introduction

Zeolites are crystalline aluminosilicate minerals with voids having dimensions in a molecular size range scale (Corma 2003). Important aspects of zeolite structures are evenly distributed pores with uniform size dimensions, high surface area, ion exchange properties, thermal stability, acidity and the ability to adsorb molecules and ionic species within the porous system of their structure. This set of attractive properties makes zeolites the object of a very wide range of applications, such as molecular sieves, ion exchangers, catalysts, often as the acid catalysts (Barrer 1982; Perez-Escobedo *et al*., 2016; Yocupicio *et al*., 2017; Torres-Otáñez *et al*., 2017). Besides of these common applications, zeolite materials can stabilize ultra-small (< 1 nm) ligand-free uniform sized clusters of foreign materials into zeolite voids (Goel *et al*., 2012; Jaime-Acuna *et al*., 2014; Stucky and Macdougall 1990).

* *Corresponding author. E-mail*: chayo_yocu@hotmail.com
doi: 10.24275/uam/izt/dcbi/revmexingquim/2018v17n3/Yocupicio
issn-e: 2395-8472

These clusters and/or nanoparticles can be applied to develop optoelectronics, sensors, drug delivery materials, etc. (Dubov *et al*., 1995; Hanrath 2012; Kim and Yoon 2014). At present, heterogeneous catalysis is the most extensive field of use of zeolites among their numerous applications. More than 40% of solid catalysts in the existing chemical industry are zeolites; nowadays catalysts constitute 27% of the global world market of zeolites (Rinaldi and Schuth 2009; Yilmaz and Muller 2009). Both mordenite and ZSM-5 are among the most used in the chemical industry, and both form a key role in novel applications. The reasons for such close attention are that these types of zeolites belong to the so-called "big five" - the five zeolites most used in industry as the catalysts (Vogt *et al*., 2015). Therefore, there is a constant interest in a detailed study of the preparation of such materials, especially to methods that allow controlling the tuning of their properties.

Synthesis of some zeolite catalysts requires the use of organic agents, or organic structure-directing agents (SDA). The ZSM-5 (Accepted by International Zeolite Association Framework Type Code for this zeolite is MFI) is usually synthesized in the presence of tetrapropylammonium salts, the generally accepted organic SDA for ZSM-5 zeolite (L. W. Beck and Davis 1998). The structure of mordenite (Framework Type Code is MOR) can be obtained using TEA^+ and neopentylamine as organic SDA (Lok *et al*., 1983). In the literature, it was reported that without the use of an organic SDA in the reaction mixture, a number of materials coexist in the resulting product, such as mordenite, ZSM-5, analcime, and quartz; their relative fraction depends on the composition, temperature and crystallization time (Ames 1963; Joshi *et al*., 1992; Shiralkar and Clearfield 1989). This happens because, in the absence of an organic SDA, these zeolite structures crystallize in a similar composition field (Aiello *et al*., 1987; Belussi *et al*., 1988; Shiralkar and Clearfield 1989), indicating that a very small change in the gel composition can shift the balance in favor of one or another particular structure (Dutta *et al*., 1994).

Despite widespread use, zeolites possessing pores in the sub-nanometer range have sufficient problems with diffusion limitations. The discovery of mesoporous silica opened the door for new materials, which would eliminate diffusion constraints for the use in the catalysis of bulky molecules. The most notorious mesoporous materials that have been synthesized using cationic surfactants are lamellar (MCM-50), hexagonal (MCM-41) or cubic (MCM-48) phases. Such a mesoscopic arrangement is interesting for a lot of applications because of its long-range ordered periodic mesostructure, but it lacks short-range order, which is a characteristic zeolite feature and which is responsible for their outstanding properties.

To solve this problem, attempts have been made to crystallize the amorphous wall of mesostructured silica by applying an organic SDA in the reaction mixture, but this has led to traditional zeolites, mesoporous amorphous materials, or a mixture of segregated phases (J. S. Beck *et al*., 1994; L. M. Huang *et al*., 2000; Karlsson *et al*., 1999). These results stimulate the search for methods that would allow the synthesis of mesoporous zeolites, which are usually called hierarchical zeolites (Moller and Bein 2013). The design (Juarez-Moreno *et al*., 2014) of advanced nanomaterials for "hierarchical organization" means to obtain a structural order of different pore scale (Holm *et al*., 2011; Mitchell *et al*., 2015; Perez-Ramirez *et al*., 2008; Lopez-Orozco *et al*., 2011).

Cetyltrimethylammonium bromide (CTAB) is a well-known agent that generates mesopores in silica (Gorelikov and Matsuura 2008; Kresge *et al*., 1992). There are some reports that in the presence of CTAB, nanozeolite MFI and hierarchical MFI and LTA can be synthesized (Chen *et al*., 2010; Hasan *et al*., 2012; Naik *et al*., 2002). A new insight into the role of CTAB in the formation of microporous and mesoporous zeolites was proposed in Ref. (Xu *et al*., 2014). However, this method often fails to generate mesopores in zeolite materials; preferentially it tends to generate mesoporous silica, rather than aluminosilicates (Karlsson *et al*., 1999; Shetti *et al*., 2008; Xia and Mokaya 2004). Progress is needed in the synthesis of hierarchical zeolites that will facilitate the emergence of new applications (Zaarour *et al*., 2014). Otherwise, the system CTAB-PEG has been used to generate mesoporous zeolites with the MFI structure. It has been proposed that the CTAB forms a micelle, while the PEG has a scaffold function between zeolites units and CTAB micelles. In this sense, PEG suffers from glycolysis around CTAB micelle (Chen *et al*., 2010). Currently, only a few studies have been reported that have received hierarchical mesophases with short-range order, typical for zeolite materials. Christiansen *et al*. reported on the preparation of molecularly ordered inorganic framework during the synthesis of silicate-surfactant mesophases (Christiansen *et al*., 2001). These lamellar mesophases were obtained by varying the charge density of the hydrophilic head-group surfactants and the time of hydrothermal synthesis. Wang *et al*. conducted a further analysis

of the system and concluded that the most important factors affecting the formation of mesophases are the temperature and composition of the gel for synthesis (Wang and Exarhos 2003). Furthermore, Mokaya group (Mokaya 2001) found that increasing the time of hydrothermal synthesis at high temperature (150 oC) can lead to the formation of crystalline nanodomains on the pore walls; in addition, soft oxidation of the surfactant by H_2O_2 at room temperature, was applied, which led to the formation of lamellar surfactant-free mesophases (Xia and Mokaya 2006). Choi *et al*. (Choi *et al*., 2006) reported on the synthesis of hierarchical zeolitic mesoporous materials that retained their crystallinity; when synthesized, a supramolecular assembly of amphiphilic surfactants was used, which were suitably functionalized by the silane group to anchor the zeolite framework. Later, Zhang *et al*., reported the formation of ZSM-5 zeolite with lamellar ordering (K. Zhang *et al*., 2009); recent findings of Messinger *et al*. indicate the coexistence of intermediate nano-layered silicates and nanosheets of ZSM-5 zeolite in the same particle (Messinger *et al*., 2015).

The aim of the present work was to study the influence of the concentration of a typical organic SDA agent for the ZSM-5 zeolite synthesis (TPABr), and the alkalinity of the synthetic mixture, in the presence of a combination of mesopore-directing agents (PEG and CTAB) on the growth of a hierarchical structure in the ZSM-5 material.

2 Materials and methods

2.1 Synthesis

The synthesis of materials in the present work is an adaptation of the methodology proposed by Shetti *et al*. for the synthesis of hierarchical MFI zeolite (Shetti *et al*., 2008). This methodology was modified: [3-(trimethoxysilyl)propyl] dodecyldimethylammonium chloride, originally used as a mesopore-directing agent, was replaced by polyethylene glycol 20000 (PEG) and cetyltrimethylammonium bromide (CTAB). The concentrations of Al_2O_3, SiO_2 and H_2O were maintained the same and constant, while the concentrations of NaOH, H_2SO_4, and TPABr were varied. For this synthesis, tetrapropylammonium bromide (TPABr) was selected as the organic structure-directing agent (SDA). All reagent grade reactants were supplied by Sigma-Aldrich.

Before starting the synthesis, silicate and aluminate solutions were prepared separately. Sodium silicate solution contains 25 wt.% of SiO_2 and 10.6 wt.% of Na_2O. Sodium aluminate solution was prepared dissolving 0.48 gr of $NaAlO_2$ in 26.6 gr of H_2O. For the hydrothermal synthesis of the first sample, labeled as M1, we prepared the mixture of 3.123 gr of CTAB, 0.5205 gr of PEG 20000, 2.66 gr of TPABr, and 0.47 gr of NaOH, completely dissolved in 36.3 ml of H_2O. Then 21.46 gr of sodium silicate solution was added and the mixture was vigorously stirred for 20 minutes. After that, a solution of sodium aluminate was added dropwise. Finally, 26 g of a 10 wt.% H_2SO_4 solution was added under vigorous stirring.

Eight mixtures for synthesis, with varying concentrations of TPABr, PEG, CTAB, sodium hydroxide and sulfuric acid were prepared in a similar way, while Al_2O_3, SiO_2 and H_2O molar contents were maintained constants. Their molar compositions are shown in Table I. These mixtures were heated at 150 ºC for 4 days in a Teflon-coated stainless steel autoclave under autogenous pressure. After that, all samples were filtered and washed with distilled water, followed by washing with methanol under refluxing for 12 hours at 60 C to remove physically occluded surfactants. Finally, they were calcined at 550 ºC for 4 hours.

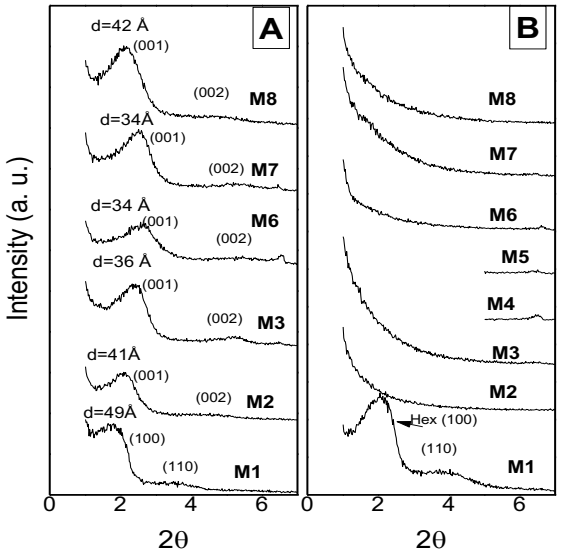

Fig. 1. XRD patterns in the low-angle range of as synthesized before calcination (A) and calcined (B) samples.

2.2 Characterization

Elemental analysis of the samples by EDS was carried out in a Jeol JSM-5300 instrument. X-ray diffraction patterns of the samples were obtained using a Philips X Pert apparatus applying Cu K_α radiation (λ = 0.154056 nm). Diffractograms were compared with the reference crystallographic database tables (ICDD). Measurements of N_2 adsorption were performed in a Micromeritics 300 equipment in order to calculate the surface area and the textural properties; Specific surface areas (SBET) were estimated by the BET (Brunauer-Emmett-Teller) method by analyzing adsorption data in the relative pressure (P/P_0) range of 0.068-0.316. The total pore volumes (V_p) were estimated from the adsorbed amount at a relative pressure (P/P_0) of 0.969. The surface of micropore (S_{micro}) and micropore volume (V_{micro}) were calculated by the t-plot method at the relative pressure range of 0.067-0.257. The samples were previously degassed at 300 °C under vacuum. The morphology and structure of the synthesized samples were determined by TEM measurements using a Jeol 2010 instrument. The quantification of present phases was performed by Rietveld refinement by using the software MAUD (Matthies *et al*., 1997).

3 Results and discussion

3.1 X-Ray Diffraction

3.1.1 As synthesized materials

Low-angle peaks are important for the characterization of regular mesoporosity, so measurements began with 2θ = 1°. Indeed, broad peaks belonging to mesostructured materials (Figure 1A) were observed, with interplanar distances in the range of 34-36 Å for samples M3, M6 and M7, and 49 Å, 41 Å and 42 Å for M1, M2 and M8 samples respectively. For M1, M2, and M3 materials, with an increase of H_2SO_4 amount (Table I), the interplanar distances of mesoporous phases are increasing too. Low angle diffraction peaks of M3, M6, and M7 samples, indexed as (001) reflections are similar to those reported to 00ℓ reflections which are associated with the lamellar mesoscale organization of the material (Brouwer *et al*., 2013; Hedin *et al*., 2004; Wang and Exarhos, 2003). Wide and low-intense peak at 2θ around 5 degrees (see Figure 1A), belongs to second order 00ℓ reflection (002) of lamellar mesostructure, while (003) reflections are undetectable due to their low intensity (see Figure 1B) (Brouwer *et al*., 2013; Hedin *et al*., 2004; Wang and Exarhos 2003).

3.1.2 Calcined materials

The low-angle part of XRD patterns of the same samples after calcination is shown in Figure 1B. Except for the M1 sample, low angles peaks are lost. The ordered mesoporous structures disappear upon calcination (with the exception of sample M1), most likely, by topotactic condensation (McNaught and Wilkinson, 1997). Nevertheless, mesoporosity is well developed (see Surface results later, Table IV), probably due to the formation of disordered materials or non-congruent collapse after withdrawal of organic material by oxidation (Roth and Cejka, 2011) of the prepared lamellar materials with the formation of amorphous mesostructured materials.

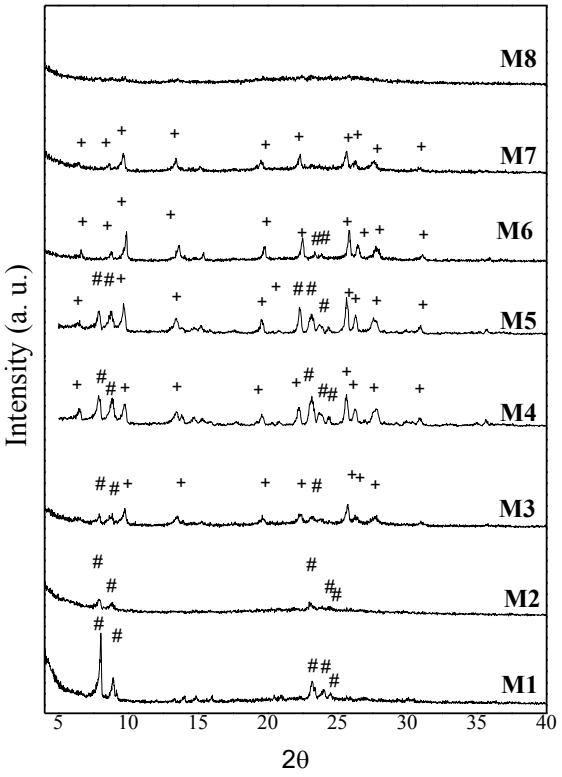

Fig. 2. XRD patterns of calcined materials obtained by varying the amounts of organic additives and mineralizer in the reaction mixture (Table I). The characteristic peaks of ZSM-5 (ICDD 00 044 0003) are labeled by the signs "#", and those of mordenite (ICDD 00 049 0924) are indicated by the "+" signs.

Table 1. Compositions of mixtures for sample preparation (mmoles). The molar compositions of the components SiO_2=94.1, Al_2O_3=3.1 and H_2O=4639, as well as the Si/Al ratio of 15 were kept constant for all samples.

Sample	CTAB	PEG	TPABr	Na_2O	H_2SO_4	Na_2O/SiO_2
M1	8.5	0.026	9.9	51.0	36.8	0.54
M2	8.5	0.026	9.9	51.0	26.4	0.54
M3	8.5	0.026	9.9	51.0	15.8	0.54
M4	8.5	0.026	11.9	57.6	26.4	0.61
M5	8.5	0.026	15.5	62.8	26.4	0.67
M6	8.5	0.026	0.0	62.8	26.4	0.67
M7	8.5	0.052	0.0	62.8	26.4	0.67
M8	16.9	0.026	0.0	62.8	26.4	0.67

In the M1 sample low angle peaks are shifted to higher diffraction angles (due to decreasing of the interplanar distance from 49 Å to 42 Å). This may be due to some reconstruction of the mesostructure during calcination, but a detailed study of all these effects is beyond the scope of the present work and will be published elsewhere. The high-angle range of XRD patterns of all obtained materials after calcination is shown in Figure 2. The M1 and M2 samples contain only MFI structure and show signals at 2θ angles of 7.904, 8.809, and 23.10, corresponding to (101), (020), and (051) reflections, respectively (see Figure 2).

Additives for mesoporosity generation used in this work diminish the crystallinity of obtained materials, in comparison with the data of Shetti *et al*., (Shetti *et al*., 2008). This can be explained by the use of two or more organic SDA agents in the same synthesis gel, which can lead to competitive interaction instead of cooperative interaction and, as a result, give some amorphous mesoporous materials, less crystallized zeolitic material, bulk zeolites without mesoporosity, or physical mixtures of all the above-mentioned phases (Choi *et al*., 2006).

Samples M3, M4 and M5 were prepared with a decreased amount of H_2SO_4 (M3 with regard to M2) or with increased concentration of NaOH and TPABr (see Table I for details). This variation of gel composition resulted in the suppression of the directed growth of the MFI structure in the presence of the selected for this purpose SDA, and, surprisingly, the crystallization of mordenite structure simultaneously with the growth of MFI was observed (Fig. 2). Typical signals are detected in 2θ angles of 9.81, 22.49, and 25.83, corresponding to (200), (240), and (202) reflections respectively of the MOR structure. With an increase in the concentration of NaOH (sample M5), an increase in the amount of crystalline MOR was observed. Together with the changes of the relative ratio of MFI/MOR products in the mixture, the unit cell parameters varied systematically (see Table II). Reference cell parameters for both zeolites are taken from database of zeolite structures (Baerlocher and McCusker 1996). The XRD patterns of M3, M4, M5, M6 and M7 samples show low contribution of (hk0) MOR planes, especially the (110) plane reported as the strongest signal in this structure (Baerlocher and McCusker 1996). This effect could indicate that these planes present a low rate of growth, due to restrictions imposed by surfactant adsorption on them. The reason for this effect is not clear and requires additional independent studies.

Several factors can influence the growth of MFI and MOR zeolites: the increase of alkalinity, the Na/Si ratio, the presence of organic agents and the crystallization time. In this case, the formation of two zeolite structures can be a consequence of the increase in alkalinity, due to NaOH addition in the synthetic mixture. Similar results reported by Shiralkar (Shiralkar and Clearfield 1989) showed the coexistence of two zeolite phases and α-quartz in the resulting synthetic material, depending on the Si/Al ratio, concentration of salts and basicity of the solution.

For concentrations similar to those used in this study, MFI and MOR mixed phases were obtained, showing higher relative quantity of MOR structure at a higher Na^+ concentration (Shiralkar and Clearfield 1989). As it is marked for the M4 and M5 samples, the appearance of MOR structure was due to the increase in the concentration of Na^+ ions that caused the displacement of phase equilibrium and preferential growth of MOR structure in comparison with the growth of MFI.

Table 2. The unit cell parameters and its volume, calculated from XRD data for calcined samples. Data for MFI and MOR standard samples with symmetry groups Pnma and Cmcm respectively are taken from (Baerlocher and McCusker 1996).

	Parameter				
	sample	a (Å)	b (Å)	c (Å)	Volume ($Å^3$)
MOR	M1	19.83	20.32	13.22	5323.6
	M2	20.05	19.93	13.29	5313.0
	M3	19.96	19.92	13.47	5355.0
	M4	19.96	19.89	13.59	5398.0
	M5	20.05	19.96	13.44	5379.2
	M6	-	-	-	-
	M7	-	-	-	-
	M8	-	-	-	-
MFI		19.88	20.11	13.37	5343.7
MOR	M1	-	-	-	-
	M2	-	-	-	-
	M3	18.12	20.40	7.48	2763.5
	M4	18.20	20.45	7.51	2792.7
	M5	18.31	20.42	7.50	2802.8
	M6	17.90	20.24	7.46	2705.1
	M7	18.35	20.37	7.49	2797.8
	M8	-	-	-	-
MOR		18.11	20.53	7.53	2798.9

The Na/Si ratio is the important parameter that influences the structure of the final crystalline product. It was also shown by Shiralkar (Shiralkar and Clearfield 1989) that the process of transformation between MFI and MOR could be controlled by changing the overall Na_2O/SiO_2 ratio in the synthetic solution. The Na_2O/SiO_2 ratio of about 0.18 is the boundary between the formation of MFI and MOR phases. Below this value, only the MFI structure was obtained, while MOR with needle morphology is formed above the Na_2O/SiO_2=0.22 ratio. It should be recalled that these values were obtained by synthesis from a completely inorganic system without the aid of organic SDA's.

In the present study, in the presence of several organic compounds, the average values of Na_2O/SiO_2 ratio changes from 0.54 (M2) which shows only the MFI structure, up to 0.67 value (M6 and M7 samples) with exclusively MOR structure.

The crystallization time used in present study was greater than that reported by Huang et al (Huang *et al*., 2012), and we got bigger relative amount of MOR phase in the obtained mixture (see Table III), and this amount increases with higher Na^+ content.

Thus, the formation of two zeolites (MFI and MOR) in the reaction mixture intended exclusively for MFI synthesis is sensitive to the concentration of Na^+ in the mixture. This occurs probably because both zeolites are formed from the same secondary building units (SBU 5-1). A similar effect was observed in the case of the inter-zeolitic conversion of MFI to the structure of β-zeolite (BEA) (Sano *et al*., 2013). Thus, the Na^+ ion plays a key role in regulating the phase equilibrium in zeolites.

The coexistence of both zeolite structures in M4 and M5 samples is linked to parameters of synthesis, such as alkalinity, the presence of CTAB and PEG, and the concentration of TPABr in synthesis solutions. Alkalinity is perhaps the most important parameter when surfactants are used in synthetic solutions. With a high surfactant concentration, it is more likely that the surfactant will be ordered in micelle arrangements that form mesoporous amorphous structures; however, these micelles can be destroyed by the action of alkalinity. In this case, individual surfactant entities are typically located within the cavities of the microporous structure, as suggested by Huang *et al*. (L. M. Huang *et al*., 2001). Thus, in the case of M6 and M7 samples, after withdrawing of TPABr from the synthetic mixture, the MOR structure was preferably formed, and although the samples showed a lower crystallinity as compared to M4 and M5, these samples (M6 and M7) displayed the diffraction peaks of MOR structure. It is interesting to note that M7 sample seems to be not affected by doubling PEG concentration, yielding MOR structure similar to M6 sample.

Finally, doubling the initial amount of CTAB results in a completely amorphous mesoporous material (sample M8), whose XRD pattern did not show the diffraction signals of the crystalline material, except for the broad signal of the amorphous material at 2θ = 16-30º. Such features of M8 are a clear consequence of the high concentration of the CTA^+ ion, resulting in a large number of lamellas, which gives a small opportunity to grow a bulk zeolitic structure and cause the formation of a laminar two-dimensional structure.

3.2 Energy Dispersive Spectroscopy (EDS)

The EDS results are summarized in Table III. In general, it is evident that for samples M1-M3, the Si/Al ratio is reduced by decreasing the H_2SO_4 content (Table III). In other words, the Si/Al ratio decreases with increasing alkalinity of the solution.

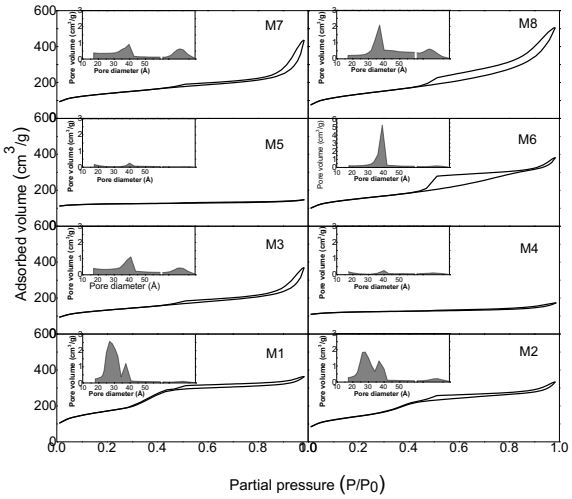

Fig. 3. Adsorption-desorption N_2 isotherms and pore distribution (inset) of calcined samples.

A typical MOR structure crystallizes with a Si/Al ratio equal to 5.0 (Baerlocher and McCusker 1996). It has been reported that the optimum gel composition for the synthesis of a typical MOR has Si/Al ratio in the range of 4 to 6 (Bajpai 1986). The MFI structure crystallizes over a wide range of Si/Al ratios from 2.55 to infinity (Baerlocher and McCusker 1996).

Samples M1 and M2 show a Si/Al ratio similar to that of the initial gel composition, which was selected for fully MFI synthesis (Shetti *et al*., 2008). On the other hand, it should be noted that samples M6 and M7 with a MOR structure grown with a non-typical for MOR high Si/Al ratio of 11.03 and 11.4, respectively, forming MOR with aluminum deficiency. This is due to the lower amount of Al available in the synthesis mixture, taking into account that the ratio of the original gel was optimized for the MFI synthesis and is equal to 15 as can be seen in Table I.

An important consideration is that a good correlation can be observed between the alkalinity of the synthetic solution and the aluminum content in the final structure of the samples (Hamidi *et al*., 2003). In this regard, it should be noted that samples M1 and M2 have a Si/Al ratio, which is very close to that in the initial gel composition. Simultaneously with the appearance of the MOR phase in the synthesis products (samples M3, M4 and M5) due to increasing in alkalinity, the Si/Al ratio decreased (see Table III). For M6 and M7 samples containing MOR, their Si/Al ratio also decreases below the initial concentration in the starting gel, although not so much as for samples M3 and M5 in which a mixture of two phases is obtained. However, it is important to note that their Si/Al ratio is more than twice as high as for a typical MOR, which is equal to 5, indicating that the resulting MOR is aluminum deficient. Finally, sample M8 shows a high Si/Al ratio of 31.2, which indicates that the amorphous phase has a more siliceous character than other synthesized materials.

It is known that the lattice parameters depend on the Si/Al ratio. A higher number of Al atoms in the unit cell increases lattice distances and cell volume, since Al-O bonds are longer than Si-O bonds (Tianyou and Ruren 1990). Table II lists the unit cell parameters of all samples, calculated from XRD data of calcined samples.

Comparing the data in Table II and Table III, it can be said that although samples M4 and M5 have a lower Si/Al ratio than the M3 sample, there is no significant variation in the unit cell volume, while sample M6 shows a significant decrease in its volume.

Table 3. Compositions of mixtures for sample preparation (mmoles). The molar compositions of the components SiO_2=94.1, Al_2O_3=3.1 and H_2O=4639, as well as the Si/Al ratio of 15 were kept constant for all samples.

	At %				
Sample	Al	Si	O	Si/Al ratio	Structure quantification by Rietveld refinement
M1	1.92	31.65	66.41	16.48	MFI (100%)
M2	2.12	31.56	66.31	14.84	MFI (100%)
M3	3.59	29.9	66.42	8.33	MOR(71.5%)/MFI(28.5%)
M4	2.89	30.92	66.19	10.69	MOR(52.8%)/MFI(47.2%)
M5	3.23	30.64	66.13	9.49	MOR(62.2%)/MFI(37.8)
M6	2.81	30.99	66.2	11.03	MOR (100%)
M7	2.64	30.2	67.08	11.44	MOR (100%)
M8	1.44	45.03	53.03	31.27	Amorphous

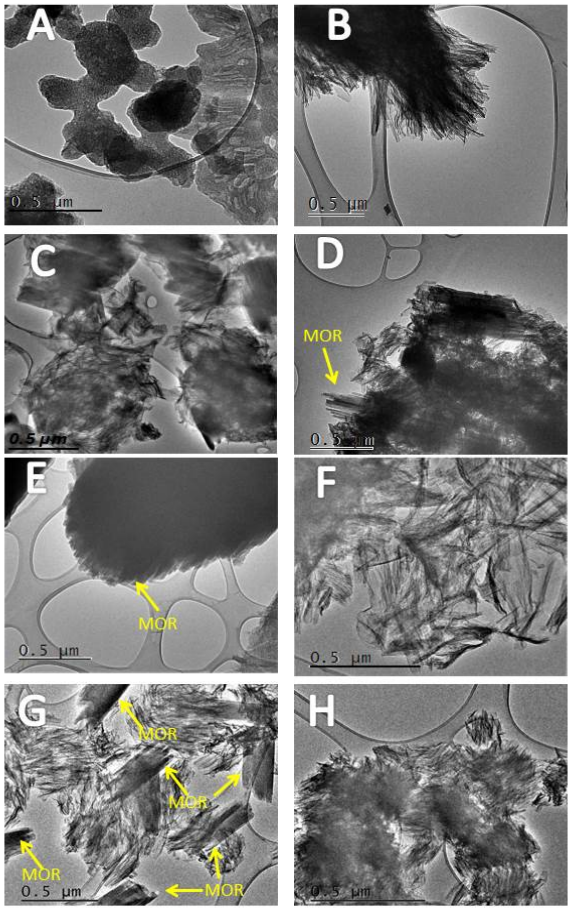

Fig. 4. Low resolution TEM micrographs of calcined samples: A – M1; B – M2; C – M3; D – M4; E – M5; F – M6; G – M7; H – M8.

This may be due to the fact that in M6 sample, the only structure is MOR. The growth of MOR requires more Al than MFI, but the synthetic mixtures used do not have enough Al, therefore, the sample undergoes a unit cell contraction.

3.3 Nitrogen physisorption, BET

Adsorption-desorption isotherms of N_2 for all samples are shown in Figure 3. Samples M4 and M5 show type I isotherms, which is typical of microporous materials. This observation is consistent with a high crystallinity of the samples shown by XRD analysis. The isotherms for the remaining samples (M1, M2, M3, M6, M7, and M8) are representatives of type IV isotherm; sample M6 shows an isotherm typical of a material with a laminar structure of flexible pores (H3), while the rest are typical for materials with a slit form mesopores (H4).

With the exception of M4 and M5, all samples exhibited adsorption at high partial pressures, revealing a textural porosity coming from the voids between the particles (Tanev and Pinnavaia 1996). Nitrogen uptake at a low relative pressure indicates that adsorption occurs within the zeolite micropores. With the exception of samples M4 and M5, all materials show significant N_2 uptake at middle relative pressure (at P/P_0= 0.4-0.45), due to the presence of mesopores.

The textural properties of the obtained materials are collected in Table IV. The data show that the surface area (SBET) decreases through the samples till M4 and M5 and then again starts to increase. This decrease of SBET can be a consequence of the increase of crystallinity while the increase for the M6, M7 and M8 samples would in turn be linked to the mesostructure enhancement.

The M1 sample was the only one to keep structured mesoporosity after calcination. For other samples, only disordered mesoporosity exists after calcination. Micropore volume Vmicro of the M3 sample is higher than that of M2; simultaneously XRD data indicate a change in the structure and appearance of the MOR phase mixed with MFI one. Crystallinity of this M3 sample is better than for M2. The micropore volume of M2 sample is barely noticeable, which corresponds to its very low crystallinity. The micropore volume continues to increase till M5 sample, and then begins to fall. Samples M4 and M5 show a remarkable decrease in the surface area SBET and total pore volume VP due to higher crystallinity as a result of an increase in crystal growth rate due to increased alkalinity (Barrer 1982; Sharma and Tomar 2011).

On the other hand, samples M6 and M7 present textural properties similar to M3 sample; these materials also show a high surface area and large pore volumes. In sample M8, the largest pore volume was presented in accordance with the mesoporous character shown by XRD.

3.4 Transmission Electron Microscopy

In general, the morphology of the samples in Figure 4 is typical of nanolaminar or flake-like materials (Rodrigues *et al*., 2015; Barakov *et al*., 2017), and in some of them, where concentrations of NaOH (M4 and M5), or PEG (M7) have been changed, well-defined crystals can be seen.

Table 4. Textural properties of calcined zeolitic materials.

Sample	S_{BET} (m^2/g)	S_{Micro} (m^2/g)	V_P (cm^3/g)	V_{Micro} (cm^3/g)
M1	606	76	0.54	0.033
M2	545	24	0.54	0.007
M3	434	138	0.49	0.076
M4	371	287	0.28	0.160
M5	376	311	0.23	0.170
M6	509	122	0.55	0.067
M7	456	122	0.55	0.067
M8	471	23	0.72	0.011

Sample M1 (Figure 4A) shows a material with a vesicular morphology that changes in samples M2 and M3 (Figures 4B and 4C) showing materials with nanosheet and nanotubular arrangements. These changes in the morphology of the M1, M2, and M3 samples appear to be related to a change in pH in the synthesis solution. Cai *et al*. and Lai *et al*. (Cai *et al*., 2001; Lai *et al*., 2014) suggest that increasing the pH in a synthesis solution can alter the morphology of the pores from the wormhole to the highly ordered MCM-41. Conversely, a lowering of pH can change the lamellar morphology to a more disordered wormhole.

Starting with sample M4, the amount of H_2SO_4 is kept constant, while the amount of NaOH in the synthesis mixture increased. This leads to an increase in the ratio of Na_2O/SiO_2 and pH. In addition, significant changes in the TPABr concentration were made (Table I). So, the growth of MFI structure was expected. Surprisingly, the micrographs for M4 and M5 samples present bunch of nanorods, that are typical for synthetic MOR (Hamidi *et al*., 2003; Jaime-Acuna *et al*., 2014; Sharma *et al*., 2008; Tang *et al*., 2013; L. Zhang *et al*., 2009). This observation confirms the XRD data (Fig. 2 and Table III). Analysis of N_2 adsorption-desorption showed adsorption in the mesoporous range, confirming that this is a mesostructured material. The difference in Na_2O/SiO_2 ratio seems to be more important for the preferred growth of MOR, although the composition of the synthetic mixture is developed for the synthesis of MFI. A simultaneous increase in the concentration of an organic SDA cannot impose obtaining of the MFI structure. Thus, sample M6 grows with the structure of the pure MOR phase. It is prepared in the absence of any organic SDA for the growth of MOR, as well as with the composition of the reaction mixture and the addition of SDA, intended solely for the synthesis of MFI. The resulting MOR sample differs only in the Si/Al ratio, which is very far from the MOR standard. Most probably, the preferential growth of MOR is a consequence of an increase in alkalinity caused by an increase in the NaOH concentration and the Na_2O/SiO_2 ratio (Table I), which coincides with the results of (Huang *et al*., 2012).

The M6 and M8 morphology present very similar features (Figures 4F and 4H). Such morphology is typical for materials growing with 2D arrangement or nanosheets (Xia and Mokaya 2006; K. Zhang *et al*., 2009). It coincides with the amorphous structure of M8 sample (Figure 2 and Table III).

The M7 sample, in addition to the morphology similar to the shown in samples M6 and M8, also showed bulk particles of MOR (Figure 4G), similar to the bunch of nanorods shown in samples M4 and M5 (Figures 4D and 4E). Bulk MOR in M7 may be the result of an increase in the concentration of PEG, since more PEG can cause glycolysis of a higher amount of CTAB micelles, keeping them packed and unavailable to interact with silicate ions to build an organic-inorganic arrangement (Chen *et al*., 2010).

The nanostructure of sample M4 can be seen in Figure 5B where two images with lattice planes are shown. Figure 5B (left side) shows the interface between two parallel nanorods of the MOR sharing planes with d = 8.9 Å, similar to the interplanar distance d = 9 Å of (200) planes of MOR (ICDD 49-0924).

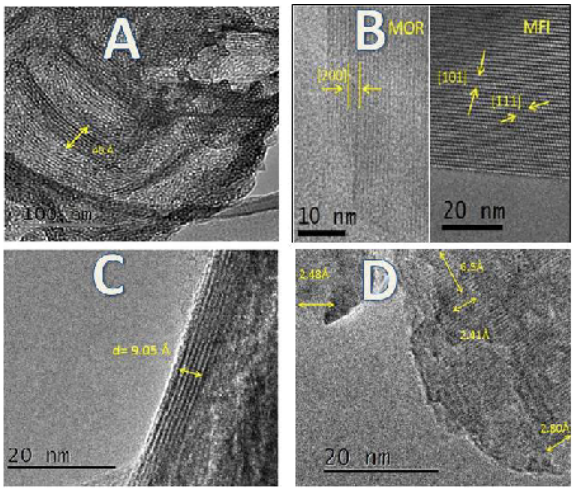

Fig. 5. High-resolution TEM micrographs of calcined samples: A – M1; B – M4; C – M6; D – M8, showing crystallographic phases and planes. Micrograph of M1 sample shows the details of mesostructure (40 Å) while micrograph of M8 sample shows the short-range molecular order within the silicate sheets [44].

Figure 5B (right side) shows a crystal of MFI in M4 sample with interplanar distances corresponding to (111) and (101) diffraction planes for the MFI orthorhombic structure. These results confirm the results of X-ray diffraction that showed the presence of both types of zeolites in the sample M4. The TEM image of the M6 nanostructure is shown in Figure 5C. The diffraction planes with 9 Å interplanar distance that corresponds to (200) plane in MOR structure are seen in that micrograph.

The observed morphology of the samples is in accordance with the XRD results. This morphology corresponds to the assumption that we obtain amorphous mesoporous materials with crystalline zeolite domains. It can be assumed that the zeolite crystal domains are located between lamellae mesopore silica, as recently proposed by Messinger *et al*. for crystallization of MFI (Messinger *et al*., 2015).

Conclusions

The original recipe for the synthesis of the MFI zeolite was modified by the addition of mesoporogen agents (CTAB and PEG) to produce a mesoporous, hierarchical material. It was found that, while maintaining the permanent silicate and aluminate concentrations of the synthetic mixture and only due to the change in alkalinity and concentration of organic SDA for the growth of MFI (TPABr), crystalline MOR zeolite begins to appear in synthesis products simultaneously with MFI. A series of samples were obtained, starting with MFI, through MFI/MOR mixtures, completely MOR-phase and finally amorphous mesoporous material. Since the synthetic mixtures used do not have a sufficient amount of Al for the synthesis of MOR framework, the Si/Al ratio of the obtained MOR phase is quite different from the typical one. The use of CTAB-PEG mixture has indeed led to the formation of a mesoporous structure (mesophase). However, along with this expected effect, it was possible to observe the appearance of the MOR structure in the composition region very far from the region of its crystallization. It can be concluded that the molar ratio of Na_2O/SiO_2 dictates the type of zeolite structure, making it clear that a particular zeolite structure (MOR) will be formed regardless of the use of an organic SDA agent destined for the growth of another zeolite (MFI).

Acknowledgements

The authors are grateful to SENER-CONACyT for financial support through Project 117373, and wish to thank E. Aparicio, I. Gradilla, E. Flores, P. Casillas, J. Mendoza and F. Ruiz for valuable technical assistance. R.I.Y acknowledges CONACyT for PhD fellowship.

References

Aiello, R., Crea, F., Nastro, A., & Pellegrino, C. (1987). Zeolite crystallization from high-silica monocatonic or bicationic alkali (Li, Na or K) gels in presence and in absence of Tpa ions. *Zeolites 7*, 549-553.

Ames, L. L. (1963). Synthesis of a clinoptilolite-like zeolite. *American Mineralogist 48*, 1374-1381.

Baerlocher, C., & McCusker, L. B. (1996). Database of zeolites structures. Available in: http://www.iza-structure.org/databases/.

Bajpai, P. K. (1986). Synthesis of Mordenite Type Zeolite. Zeolites 6, 2-8.

Barakov R., Shcherban N., Yaremov P., Bezverkhyy I., Baranchikov A., Trachevskii V., Tsyrina V., & Ilyin V. (2017). Synthesis of micro-mesoporous aluminosilicates on the basis of ZSM-5 zeolite using dual-functional templates at presence of micellar and molecular templates. *Microporous and Mesoporous Materials 237*, 90-107.

Barrer, R. M. (1982). *Hydrotermal Chemistry of Zeolites*. Academic Press, London.

Beck, J. S., Vartuli, J. C., Kennedy, G. J., Kresge, C. T., Roth, W. J., & Schramm, S. E. (1994). Molecular or supramolecular templating - defining the role of surfactant chemistry in the formation of microporous and mesoporous molecular-sieves. *Chemistry of Materials 6*, 1816-1821.

Beck, L. W., & Davis, M. E. (1998). Alkylammonium polycations as structure-directing agents in MFI zeolite synthesis. *Microporous and Mesoporous Materials 22*, 107-114.

Belussi, G., Perego, G., Carati, A., Cornaro, U., & Fattore, V. (1988). In: *Innovation in Zeolites*

Materials Science (P. J. Grobel, Ed.), pp. 37-44. Elsevier, Amsterdam.

Brouwer, D. H., Cadars, S., Eckert, J., Liu, Z., Terasaki, O., & Chmelka, B. F. (2013). A general protocol for determining the structures of molecularly ordered but noncrystalline silicate frameworks. *Journal of the American Chemical Society 135*, 5641-5655.

Cai, Q., Luo, Z. S., Pang, W. Q., Fan, Y. W., Chen, X. H., & Cui, F. Z. (2001). Dilute solution routes to various controllable morphologies of MCM-41 silica with a basic medium. *Chemistry of Materials 13*, 258-263.

Corma, A. (2003). State of the art and future challenges of zeolites as catalysts. *Journal of Catalysis 216*, 298-312.

Chen, G. D., Jiang, L., Wang, L. Z., & Zhang, J. L. (2010). Synthesis of mesoporous ZSM-5 by one-pot method in the presence of polyethylene glycol. *Microporous and Mesoporous Materials 134*, 189-194.

Choi, M., Cho, H. S., Srivastava, R., Venkatesan, C., Choi, D. H., & Ryoo, R. (2006). Amphiphilic organosilane-directed synthesis of crystalline zeolite with tunable mesoporosity. *Nature Materials 5*, 718-723.

Christiansen, S. C., Zhao, D. Y., Janicke, M. T., Landry, C. C., Stucky, G. D., & Chmelka, B. F. (2001). Molecularly ordered inorganic frameworks in layered silicate surfactant mesophases. *Journal of the American Chemical Society 123*, 4519-4529.

Dubov, P. L., Korolkov, D. V., & Petranovskii, V. P. (1995). *Clusters and Matrix Isolated Cluster Superstructures*. St. Petersburg University, St. Petersburg.

Dutta, P. K., Rao, K. M., Kresge, C. T., & Kennedy, G. J. (1994). Examination of the growth dynamics of zeolites ZSM-5 and mordenite from inorganic reactant compositions. *Microporous Materials 3*, 17-27.

Goel, S., Wu, Z. J., Zones, S. I., & Iglesia, E. (2012). Synthesis and catalytic properties of metal clusters encapsulated within small-pore (SOD, GIS, ANA) zeolites. *Journal of the American Chemical Society 134*, 17688-17695.

Gorelikov, I., & Matsuura, N. (2008). Single-step coating of mesoporous silica on cetyltrimethyl ammonium bromide-capped nanoparticles. *Nano Letters 8*, 369-373.

Hamidi, F., Bengueddach, A., Di Renzo, F., & Fajula, F. (2003). Control of crystal size and morphology of mordenite. *Catalysis Letters 87*, 149-152.

Hanrath, T. (2012). Colloidal nanocrystal quantum dot assemblies as artificial solids. *Journal of Vacuum Science & Technology A 30*.

Hasan, F., Singh, R., Li, G., Zhao, D. Y., & Webley, P. A. (2012). Direct synthesis of hierarchical LTA zeolite via a low crystallization and growth rate technique in presence of cetyltrimethylammonium bromide. *Journal of Colloid and Interface Science 382*, 1-12.

Hedin, N., Graf, R., Christiansen, S. C., Gervais, C., Hayward, R. C., Eckert, J., *et al*. (2004). Structure of a surfactant-templated silicate framework in the absence of 3D crystallinity. *Journal of the American Chemical Society 126*, 9425-9432.

Holm, M. S., Taarning, E., Egeblad, K., & Christensen, C. H. (2011). Catalysis with hierarchical zeolites. *Catalysis Today 168*, 3-16.

Huang, L. M., Chen, X. Y., & Li, Q. Z. (2001). Synthesis of microporous molecular sieves by surfactant decomposition. *Journal of Materials Chemistry 11*, 610-615.

Huang, L. M., Guo, W. P., Deng, P., Xue, Z. Y., & Li, Q. Z. (2000). Investigation of synthesizing MCM-41/ZSM-5 composites. *Journal of Physical Chemistry B 104*, 2817-2823.

Huang, X. L., Zhang, R. R., & Wang, Z. B. (2012). Controlling crystal transformation between zeolite ZSM-5 and mordenite without organic structure-directing agent. *Chinese Journal of Catalysis 33*, 1290-1298.

Jaime-Acuna, O. E., Villavicencio, H., Diaz-Hernandez, J. A., Petranovskii, V., Herrera, M., & Raymond-Herrera, O. (2014). Atomic and Electronic Structure of Quaternary $Cd_xZn_yS_\delta$ O_γ nanoparticles grown on mordenite. *Chemistry of Materials 26*, 6152-6159.

Joshi, P. N., Shaikh, A. A., Chumbhale, V. R., Rao, B. S., & Shiralkar, V. P. (1992). Crystallization of zeolite mordenite and ZSM-5 without the aid of a template. *Journal of Inclusion Phenomena and Molecular Recognition in Chemistry 13*, 171-179.

Juarez-Moreno, K., Pestryakov, A., & Petranovskii, V. (2014). Engineering of supported nanomaterials. *XV International Scientific Conference Chemistry and Chemical Engineering in Xxi Century Dedicated to Professor L.P. Kulyov 10*, 25-30.

Karlsson, A., Stocker, M., & Schmidt, R. (1999). Composites of micro- and mesoporous materials: simultaneous syntheses of MFI/MCM-41 like phases by a mixed template approach. *Microporous and Mesoporous Materials 27*, 181-192.

Kim, H. S., & Yoon, K. B. (2014). Preparation and characterization of CdS and PbS quantum dots in zeolite Y and their applications for nonlinear optical materials and solar cell. *Coordination Chemistry Reviews 263*, 239-256.

Kresge, C. T., Leonowicz, M. E., Roth, W. J., Vartuli, J. C., & Beck, J. S. (1992). Ordered mesoporous molecular-sieves synthesized by a liquid-crystal template mechanism. *Nature 359*, 710-712.

Lai, S.-M., Lai, H.-Y., & Chou, M.-Y. (2014). A facile approach for the tunable wormlike or ordered pore morphology of mesoporous silica: Effect of catalyst types and polyethylene glycol. *Microporous and Mesoporous Materials 196*, 31-40.

Lok, B. M., Cannan, T. R., & Messina, C. A. (1983). The role of organic-molecules in molecular-sieve synthesis. *Zeolites 3*, 282-291.

Lopez-Orozco, S., Inayat, A., Schwab, A., Selvam, T., & Schwieger, W. (2011). Zeolitic materials with hierarchical porous structures. *Advanced Materials 23*, 2602-2615.

McNaught A.D., & Wilkinson A. (1997). *Chemistry, Compendium of Chemical Terminology: IUPAC Recommendations, International Union of Pure and Applied chemistry*, Blackwell Science, USA.

Matthies, S., Lutteroti, L., & Wenk, H. R. (1997). Advances in texture analysis from diffraction spectra. *Journal of Applied Crystallography 30*, 31-42.

Messinger, R. J., Na, K., Seo, Y., Ryoo, R., & Chmelka, B. F. (2015). Co-development of crystalline and mesoscopic order in mesostructured zeolite nanosheets. *Angewandte Chemie-International Edition 54*, 927-931.

Mitchell, S., Pinar, A. B., Kenvin, J., Crivelli, P., Karger, J., & Perez-Ramirez, J. (2015). Structural analysis of hierarchically organized zeolites. *Nature Communications 6*, Article number: 8633.

Mokaya, R. (2001). Observation of some pore wall ordering in mesoporous silica. *Chemical Communications*, 1092-1093.

Moller, K., & Bein, T. (2013). Mesoporosity - a new dimension for zeolites. *Chemical Society Reviews 42*, 3689-3707.

Naik, S. P., Chen, J. C., & Chiang, A. S. T. (2002). Synthesis of silicalite nanocrystals via the steaming of surfactant protected precursors. *Microporous and Mesoporous Materials 54*, 293-303.

Perez-Escobedo, A., Diaz-Flores, P. E., Rangel-Mendez, J. R., Cerino-Cordova, F. J., Ovando-Medina, V. M., & Alcala-Jauregui, J. A. (2016). Fluoride adsorption capacity of composites based on chitosan-zeolite-algae. *Revista Mexicana de Ingeniería Química 15*, 139-147.

Perez-Ramirez, J., Christensen, C. H., Egeblad, K., Christensen, C. H., & Groen, J. C. (2008). Hierarchical zeolites: enhanced utilisation of microporous crystals in catalysis by advances in materials design. *Chemical Society Reviews 37*, 2530-2542.

Rinaldi, R., & Schuth, F. (2009). Design of solid catalysts for the conversion of biomass. *Energy & Environmental Science 2*, 610-626.

Rodrigues M.V., Vignatti C., Garetto T., Pulcinelli S.H., Santilli C.V., Martins L. (2015). Glycerol dehydration catalyzed by MWW zeolites and the changes in the catalyst deactivation caused by porosity modification. *Applied Catalysis A: General 495*, 84-91.

Roth W.J., Cejka J. (2011). Two-dimensional zeolites: dream or reality? *Catalysis Science and Technology 1*, 43-53.

Sano, T., Itakura, M., & Sadakane, M. (2013). High potential of interzeolite conversion method for zeolite synthesis. *Journal of the Japan Petroleum Institute 56*, 183-197.

Sharma, P., Rajaram, P., & Tomar, R. (2008). Synthesis and morphological studies of nanocrystalline MOR type zeolite material. *Journal of Colloid and Interface Science 325*, 547-557.

Sharma, P., & Tomar, R. (2011). Sorption behaviour of nanocrystalline MOR type zeolite for Th(IV) and Eu(III) removal from aqueous waste by batch treatment. *Journal of Colloid and Interface Science 362*, 144-156.

Shetti, V. N., Kim, J., Srivastava, R., Choi, M., & Ryoo, R. (2008). Assessment of the mesopore wall catalytic activities of MFI zeolite with mesoporous/microporous hierarchical structures. *Journal of Catalysis 254*, 296-303.

Shiralkar, V. P., & Clearfield, A. (1989). Synthesis of the molecular-sieve ZSM-5 without the aid of templates. *Zeolites 9*, 363-370.

Stucky, G. D., & Macdougall, J. E. (1990). Quantum confinement and host guest chemistry - probing a new dimension. *Science 247*, 669-678.

Tanev, P. T., & Pinnavaia, T. J. (1996). Mesoporous silica molecular sieves prepared by ionic and neutral surfactant templating: A comparison of physical properties. *Chemistry of Materials 8*, 2068-2079.

Tang, T. D., Zhang, L., Fu, W. Q., Ma, Y. L., Xu, J., Jiang, J., *et al*. (2013). Design and synthesis of metal sulfide catalysts supported on zeolite nanofiber bundles with unprecedented hydrodesulfurization activities. *Journal of the American Chemical Society 135*, 11437-11440.

Tianyou, S., & Ruren, X. (1990). The influence of the templating agent on the unit cell volume of ZSM-5 zeolite. *Journal of Solid State Chemistry 88*, 577-578.

Torres-Otáñez, G., Diaz de Leon, J. N., Zepeda, T. A., Pawelec, B., Fierro, J. L. G., & Fuentes, S. (2017). Preparation and evaluation of (Ni)CoMo hydrodesulfurization catalysts supported over a binary Zeolite(beta)-KIT siliceous material. *Revista Mexicana de Ingeniería Química 17*, 14.

Vogt, E. T. C., Whiting, G. T., Dutta Chowdhury, A., & Weckhuysen, B. M. (2015). Zeolites and zeotypes for oil and gas conversion. In: *Advances in Catalysis* (F. C. Jentoft Ed.), pp. 143-314: Academic Press.

Wang, L. Q., & Exarhos, G. J. (2003). Study of local molecular ordering in layered surfactant-silicate mesophase composites. *Journal of Physical Chemistry B 107*, 443-450.

Xia, Y. D., & Mokaya, R. (2004). On the synthesis and characterization of ZSM-5/MCM-48 aluminosilicate composite materials. *Journal of Materials Chemistry 14*, 863-870.

Xia, Y. D., & Mokaya, R. (2006). Crystalline-like molecularly ordered mesoporous aluminosilicates derived from aluminosilica-surfactant mesophases via benign template removal. *Journal of Physical Chemistry B 110*, 9122-9131.

Xu, D. D., Feng, J., & Che, S. A. (2014). An insight into the role of the surfactant CTAB in the formation of microporous molecular sieves. *Dalton Transactions 43*, 3612-3617.

Yilmaz, B., & Muller, U. (2009). Catalytic applications of zeolites in chemical industry. *Topics in Catalysis 52*, 888-895.

Yocupicio, R. I., de-Leon, L. N. D., Zepeda, T. A., & Fuentes, S. (2017). Study of CoMo catalysts supported on hierarchical mesoporous zeolites for hydrodesulfurization of dibenzotihophene. *Revista Mexicana de Ingeniería Química 16*, 503-520.

Zaarour, M., Dong, B., Naydenova, I., Retoux, R., & Mintova, S. (2014). Progress in zeolite synthesis promotes advanced applications. *Microporous and Mesoporous Materials 189*, 11-21.

Zhang, K., Wang, Y. M., Albela, B., Chen, L., He, M. Y., & Bonneviot, L. (2009). From ill-resolved atomic to ZSM-5 type of ordering in mesoporous lamellar aluminosilica nanoparticles. *New Journal of Chemistry 33*, 2479-2485.

Zhang, L., van Laak, A. N. C., de Jongh, P. E., & de Jong, K. P. (2009). Synthesis of large mordenite crystals with different aspect ratios. *Microporous and Mesoporous Materials 126*, 115-124.